# Interplay between Hot Carrier and Bias Stress Components in Single-Layer Double-Gated Graphene Field-Effect Transistors

Yury Illarionov, Michael Waltl, Anderson Smith, Sam Vaziri, Mikael Ostling, Max Lemme and Tibor Grasser

***Abstract*—We examine the interplay between the degradations associated with the bias-temperature instability (BTI) and hot carrier degradation (HCD) in single-layer double-gated graphene field-effect transistors (GFETs). Depending on the polarity of the applied BTI stress, the HCD component acting in conjuction can either accelerate or compensate the degradation. The related phenomena are studied in detail at different temperatures. Our results show that the variations of the charged trap density and carrier mobility induced by both contributions are correlated. Moreover, the electron/hole mobility behaviour agrees with the previously reported attractive/repulsive scattering asymmetry.**

## I. Introduction

Graphene is a superior carbon material which is considered a promising candidate for various applications in modern micro- and nanoelectronics. The main advantages of graphene compared to most traditional materials are extremely high room-temperature carrier mobility [1, 2] and saturation velocity [3]. In addition, good compatibility of graphene with complimentary metal oxide semiconductor (CMOS) technology allows to integrate this material into the standard device manufacturing processes. In particular, during the last few years, several successful attempts at fabricating graphene FETs (GFETs) [4–9] have been undertaken by different groups worldwide. These advances have created a demand for the characterization of the reliability of these devices. Despite this, only a few papers devoted to BTI in GFETs have been published recently [10–13]. At the same time, the problem of hot-carrier degradation (HCD) in GFETs has not been given any attention, although this reliability issue is known to be crucial in Si FETs [14].

In this work we study the interplay between the BTI degradation resulting from a voltage applied to the high-k top gate of double-gated GFET and the HCD associated with the application of a drain-source voltage. We show that the positive BTI (PBTI) and HCD components typically create defects of opposite signs, which leads to a non-trivial impact on the device performance if they are applied in conjuction. Investigation of the temperature dependence of the related interaction between different defects allowed us to illustrate that the resulting changes in the charged trap density and carrier mobility are correlated.

Yu.Yu. Illarionov, Michael Waltl and T. Grasser are with the Institute for Microelectronics (TU Wien), 27-29 Gusshausstrasse, 1040 Vienna, Austria
e-mail: illarionov|grasser@iue.tuwien.ac.at
Yu.Yu. Illarionov is also with Ioffe Physical-Technical Institute, Polytechnicheskaya 26, 194021 St-Petersburg, Russia
A. Smith, S. Vaziri and M. Ostling are with KTH Royal Institute of Technology, School of Information and Communication Technology, Isafjordsgatan 22, 16440 Kista, Sweden
Max Lemme is with University of Siegen, Holderlinstrasse 3, 57076 Siegen, Germany

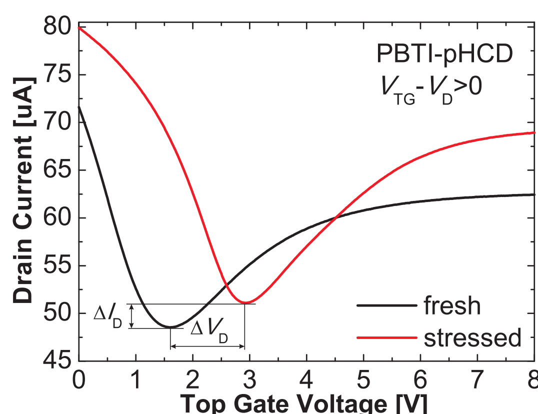


Fig. 1. The bias and HCD components applied in conjuction result in a shift of the voltage ($\Delta V_D$) and current ($\Delta I_D$) at the Dirac point. If the HCD component is significant, $\Delta I_D$ can be considerable. For this reason, the previously used definition of GFET threshold voltage introduced by the authors of [11, 13] is problematic. Therefore, we consider the degradation/recovery dynamics of BTI-HCD stress in terms of $\Delta V_D$, which allows us to correctly estimate the charged trap density shift related to the applied stress.

## II. Devices

We perform our study on single-layer double-gated GFETs fabricated using a standard lithography process [15]. In these devices 25 nm thick $Al_2O_3$ is used as a top gate insulator and 1800 nm thick $SiO_2$ is employed as a back gate insulator, while the channel lengths are $1-4\,\mu$m and widths $4-80\,\mu$m. In order to reduce device-to-device variability, the devices have been baked at $T = 300$°C in a $H_2$/He mixture [16]. Also, the performance of our GFETs is in agreement with the results published by other groups [10].

## III. Experiment

The measurements of the top gate transfer characteristics were performed in vacuum ($\sim 10^{-5}$ torr). This was necessary to enhance the reliability of our analysis by avoiding the detrimental impact of the ambient [13]. The impact of HC and bias stress on the device performance was examined as follows: after measuring the reference transfer characteristic, a stress with constant $V_{TG}$ and drain voltage $V_d$ was applied.

978-1-4673-7135-3/15/$31.00 ©2015 IEEE

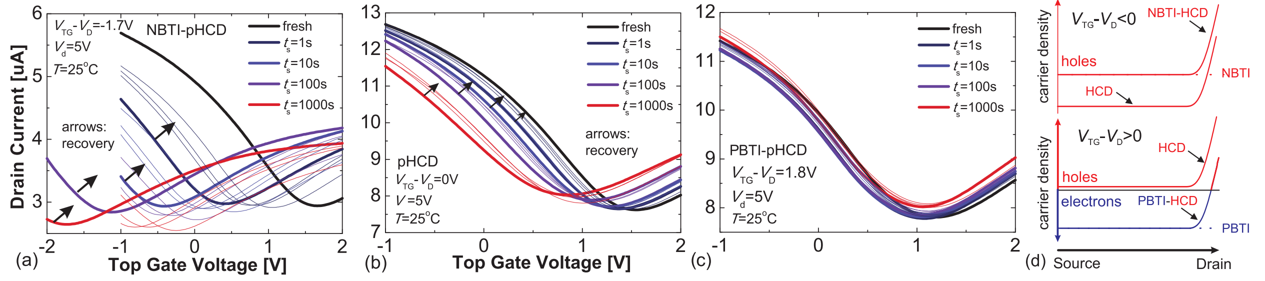


Fig. 2. Time evolution of the top gate transfer characteristics after the stresses with the same pHCD and different bias components: a) NBTI-pHCD ($V_{\mathrm{TG}}$ - $V_{\mathrm{D}} < 0$), b) pure pHCD ($V_{\mathrm{TG}}$ - $V_{\mathrm{D}} = 0$), c) PBTI-pHCD ($V_{\mathrm{TG}}$ - $V_{\mathrm{D}} > 0$). The pHC degradation has NBTI-like nature and therefore makes the NBTI degradation more severe, while compensating the PBTI degradation. d) The simulated distributions of the carrier concentration along the channel show that the pHCD component leads to an increase of hole concentration closely to the drain. Trapping of these holes introduces additional positively charged defects, which either play together with the ones created by the NBTI component or compensate the negative charges originating from PBTI. In the case of PBTI-pHCD the negatively charged defects are concentrated at the source side of the channel, while the positively charged defects are situated near the drain.

Then the recovery of the stressed device was monitored for several hours/days. For a more detailed analysis of the degradation/recovery dynamics, the measurements have been repeated with either increasing stress times ($t_{\mathrm{s}} = 1$, 10, 100 and 1000 s) or drain voltages ($V_{\mathrm{d}} = 0 ... \pm 12$ V). After each measurement, the top gate voltage was adjusted as $V_{\mathrm{TG}}$ - $V_{\mathrm{D}} \approx$ const, accounting for the shift of the Dirac point $V_{\mathrm{D}}$ after the previous stress round. This was necessary to approximately maintain a constant oxide field during all stress rounds [16].

## IV. Results and discussions

In Fig. 1 we show the typical impact of PBTI stress ($V_{\mathrm{TG}}$ - $V_{\mathrm{D}} > 0$) applied in conjuction with the positive ($V_{\mathrm{d}} > 0$) HCD component (i.e. PBTI-pHCD). Clearly, the degradation is associated with both a vertical ($\Delta I_{\mathrm{D}}$) and horizontal ($\Delta V_{\mathrm{D}}$) shift of the Dirac point and also with a transformation of the shape of the transfer characteristics. The latter typically becomes more pronounced after stress with a stronger HCD component. The observed behaviour originates from a change in the concentration of charged border traps induced by the applied stress. Obviously, this may have a considerable impact on both channel electrostatics and carrier mobility. However, the most crucial issue is that a vertical drift $\Delta I_{\mathrm{D}}$ makes the definition of the GFET threshold voltage from [11, 13] questionable, especially if a considerable HCD component is present. Therefore, we will express the degradation/recovery dynamics of BTI-HCD in terms of a horizontal shift of the Dirac point $\Delta V_{\mathrm{D}}$, which has been suggested in our previous paper on pure BTI [16]. The feasibility of this approach is also justified by the simple relation $\Delta N_{\mathrm{T}} = \Delta V_{\mathrm{D}} C_{\mathrm{ox}}/q$, which links $\Delta V_{\mathrm{D}}$ with the charged trap density shift $\Delta N_{\mathrm{T}}$.

In order to get some initial understanding on how the BTI-HCD dynamics depend on the polarity of the bias component, we have performed measurements using a fixed pHCD component $V_{\mathrm{d}} = 5$ V and three different $V_{\mathrm{TG}}$ - $V_{\mathrm{D}}$ corresponding to NBTI ($V_{\mathrm{TG}}$ - $V_{\mathrm{D}} < 0$), no bias component ($V_{\mathrm{TG}}$ - $V_{\mathrm{D}} = 0$) and PBTI ($V_{\mathrm{TG}}$ - $V_{\mathrm{D}} > 0$). The resulting time evolution of the top gate transfer characteristics is plotted in Fig. 2. Obviously, in the case of NBTI-pHCD the Dirac voltage shift towards more negative values is considerable even if the bias component is small (Fig. 2a). In addition, some vertical drift $\Delta I_{\mathrm{D}}$ is observed. The pure pHCD stress (Fig. 2b) also shifts $V_{\mathrm{D}}$ towards more negative values, although less significantly. Interestingly, in both cases the HC degradation is recoverable, contrary to Si FETs. Alternatively, a small PBTI stress accompanied by a pHC component (PBTI-pHCD) does not impact the device performance considerably (Fig. 2c). Therefore, in our GFETs the impact of NBTI stress becomes more severe, if it is accompained by a pHCD component. Conversely, PBTI degradation is reduced by an accompanying pHCD component. In order to understand this behaviour, we have performed some simulations using the drift model for GFETs reported in [17]. Since in this model the diffusion contribution is not accounted for, the obtained results are suitable only for a qualitative analysis. In Fig. 2d the simulated distributions of the carrier concentration along the channel are sketched. The pure NBTI stress acts in the hole conduction region of GFET and therefore leads to hole trapping. Contrary, the pure PBTI stress acting in the electron conduction region leads to electron trapping. At the same time, the hole/electron concentration is constant along the channel. Activation of the pHCD component increases the hole concentration closely to the drain, independently of the polarity of the bias stress. Therefore, pHCD introduces additional positively charged defects and accelerates NBTI degradation. Conversely, suppression of PBTI degradation by pHCD originates in the compensation of negatively charged defects introduced by the former by positively charged defects associated with the latter. In that case the negative charges are concentrated at the source side of the channel, while the positive charges are situated closely to the drain.

The results above show that an interaction between the defects with opposite signs should take place if the PBTI and the pHCD stress components act together. Therefore, in the context of this work, the case of PBTI-pHCD is more interesting than NBTI-pHCD. Thus, in the next experiments we fix $V_{\mathrm{TG}}$ - $V_{\mathrm{D}} = 4$ V and apply the subsequent long PBTI-pHCD stresses ($t_{\mathrm{s}} = 1000$ s) with increasing pHCD component. The resulting time evolution of the top gate transfer characteristics and corresponding $\Delta V_{\mathrm{D}}$ recovery traces measured at $T = 25°$C and $T = 120°$C are given in Fig. 3. We observe that PBTI degradation is strongly suppressed by the pHCD component Moreover, after stress with a considerable pHCD component the recovery beyond the initial Dirac voltage (i.e. over-recovery) is observed. This effect originates from the

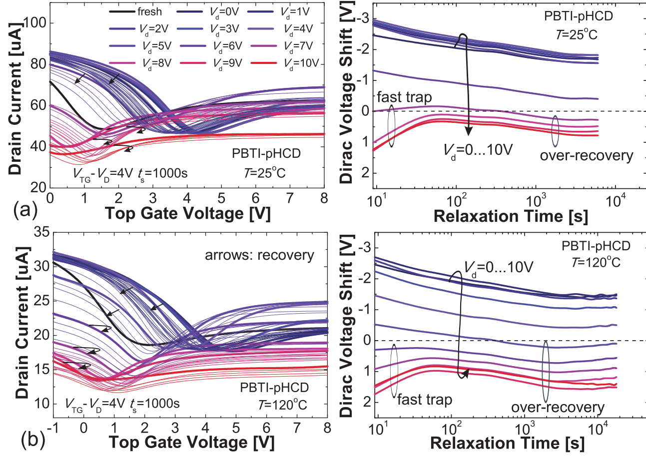


Fig. 3. Time evolution of the top gate transfer characteristics after subsequent PBTI-pHCD stress with increasing pHCD component and the corresponding recovery traces: a) $T = 25°C$, b) $T = 120°C$. In both cases PBTI degradation is compensated by the pHCD component. The latter introduces additional weakly recoverable positively charged defects which lead to over-recovery beyond the initial Dirac point and also adds an NBTI-like fast trap response. At higher temperature these effects become more pronounced, which means that the pHCD component is accelerated by temperature.

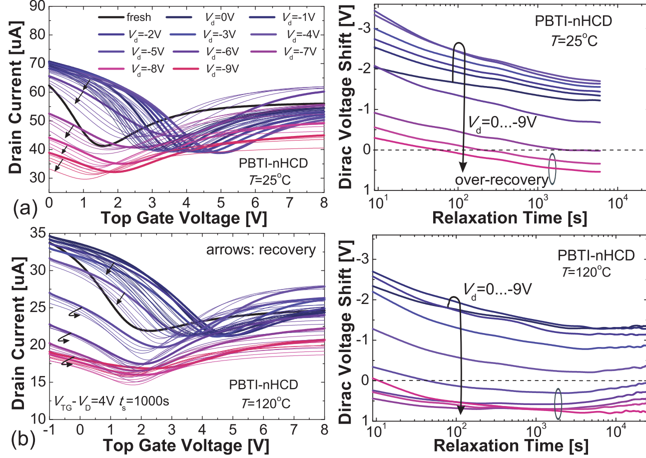


Fig. 4. Time evolution of the top gate transfer characteristics after subsequent PBTI-nHCD stress with increasing nHCD component and the corresponding recovery traces: a) $T = 25°C$, b) $T = 120°C$. At $T = 25°C$, PBTI degradation is first accelerated and then suppressed by the nHCD component, while at $T = 120°C$ the compensation takes place independently of the nHCD magnitude. Therefore, the nHCD component is able to introduce some negative charges, contrary to its pHCD counterpart. However, at higher temperature this asymmetry is significantly less pronounced.

presence of some weakly recoverable positive charges which are associated with the pHCD component. Obviously, these defects shift the initial Dirac point in an NBTI-like manner, while the negatively charged defects introduced by the PBTI component continue to recover in a PBTI-like manner. At the same time, a very strong pHCD component introduces an NBTI-like fast trap response into the recovery traces, similarly to the case of pure NBTI [16]. Comparison of the results obtained at different temperatures shows that at $T = 120°C$ compensation of PBTI degradation by the pHCD contribution becomes pronounced starting at smaller $V_d$, while NBTI-like fast traps also appear earlier. Therefore, we conclude that the pHCD component is accelerated at higher temperature.

In the next step we performed similar measurements with $V_{TG} - V_D = 4\,V$ and $V_d < 0$ (i.e. PBTI-nHCD). The results obtained at $T = 25°C$ and $T = 120°C$ are shown in Fig. 4. Contrary to the previous case, the nHCD component is able to introduce some negative charges at smaller $V_d$. This leads to acceleration of the PBTI component at $T = 25°C$. Conversely, a strong nHCD component acts in the same manner as pHCD and leads to a compensation of the PBTI degradation and over-recovery. As for the case of $T = 120°C$, the nHCD component compensates PBTI independently of $V_d$. However, NBTI-like fast traps are not present, which suggests that some asymmetry between the pHC and nHC contributions is still pronounced at $T = 120°C$.

In Fig. 5 we depict the resulting defect density shifts extracted from the recovery traces given in Figs. 3 and 4. Clearly, the asymmetry between PBTI-pHCD and PBTI-nHCD observed 10 s after the stresses at $T = 25°C$ almost disappear at $T = 120°C$ (Fig. 5a). The only conserved trend is that a strong pHCD component introduces more positive charges than the nHCD component of the same magnitude, while the difference is mainly due to NBTI-like fast traps. The related results obtained after 6000 s recovery (Fig. 5b) show that both pHCD and nHCD components of large magnitude introduce weakly recoverable positive charges. Obviously, the concentration of these defects is larger at higher temperature, leading to a stronger over-recovery (cf. Figs. 3 and 4). Also, the range of stress $V_d$ within which the charge compensation takes place is wider at $T = 120°C$. The reason for this is that not only the HC, but also the bias component becomes more pronounced at higher temperature [16]. Therefore, at $T = 120°C$ a strong interplay between the defects with opposite signs introduced by the PBTI and HCD components starts at smaller $V_d$. Analysis of the $I_d$ - $V_{TG}$ characteristics given in Figs. 3 and 4 allow us to extract electron and hole mobility at all stress/recovery phases using the method suggeste in [18]. The obtained values related to the mobilities measured before the stress are plotted versus stress $V_d$ in Fig. 6 for PBTI-pHCD and PBTI-nHCD. One can see that in both cases the electron mobility increases with respect to its initial value, which becomes more pronounced at $T = 120°C$. At both temperatures the electron mobility maximum is located within the $V_d$ range corresponding to the charge compensation region (cf. Fig. 5). This behaviour is more likely related to screening effects [19] which accompany the interplay between the defects with opposite signs. Obviously, at higher temperature the charge compensation starts at smaller $V_d$ but proceeds more slowly, making the interplay between different defects and, consequently, the electron mobility maximum more pronounced. Moreover, the relative decrease in electron mobility after the maximum is stronger than for holes. This is due to the presence of extra positively charged defects due to which electrons experience a strong attractive and holes weak repulsive scattering. Conversely, at small $V_d$, when the negatively charged defects dominate, the relative degradation of the hole mobility is stronger. Therefore, we can conclude that the mobility change associated with BTI-HCD stress not only correlates with a variation of the defect

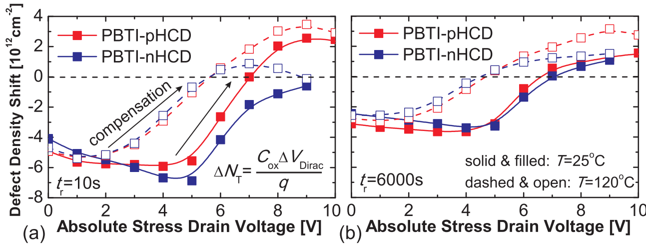


Fig. 5. Defect density shifts vs. $V_d$ for PBTI-pHCD and PBTI-nHCD at two different relaxation time points: a) $t_r = 10$ s, b) $t_r = 6000$ s. The results corresponding to $T = 25°C$ and $T = 120°C$ are plotted. At $T = 120°C$ the charge compensation region is wider and the concentration of weakly recoverable positive charges is larger. Also, the significant difference between PBTI-pHCD and PBTI-nHCD visible at $T = 25°C$, especially 10 s after the stress, becomes less pronounced at higher temperature.

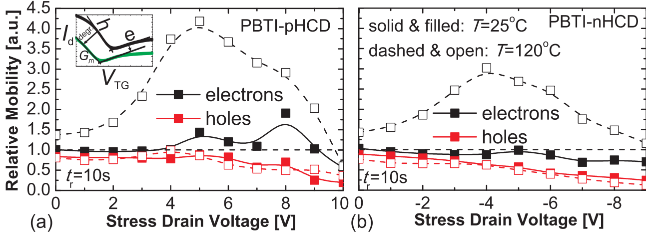


Fig. 6. Relative mobility vs. $V_d$ for PBTI-pHCD (a) and PBTI-nHCD (b) at two different temperatures. In both cases the electron mobility increases with respect to its initial value, which is likely associated with screening effects and becomes more crucial at $T = 120°C$. The position of the electron mobility maximum corresponds to the charge compensation region, which is also more pronounced at higher temperature (Fig. 5). Therefore, the mobility and charged trap density variations are correlated.

density, but also agrees with the attractive/repulsive scattering asymmetry reported in [20].

## V. Conclusions

We have performed a detailed study of the interplay between the HCD and bias stress components in single-layer double-gated GFETs. Our results show that this interplay is stronger if the HC stress acts in conjuction with PBTI. The experiments performed for this case demonstrate that at higher temperature the number of defects created by both bias and HC stress is larger and the interaction between them in terms of their charges and potentials is stronger. This impacts both charged trap density shift and mobility which are correlated. Moreover, the mobility variation agrees with the previously reported attractive/repulsive scattering asymmetry [20].

## Acknowledgment

The authors thank the EC for the financial support through the STREP projects MoRV (n° 619234) and GRADE (n° 317839), an ERC Starting Grant (InteGraDe, n° 307311), the German Research Foundation (DFG, LE 2440/1-1 and 2-1), the Swedish Research Council.

## References

[1] A.K. Geim and K.S. Novoselov, "The Rise of Graphene," *Nature Materials*, vol. 6, no. 3, pp. 183–191, 2007.

[2] K.S. Novoselov, A.K. Geim, S.V. Morozov, D. Jiang, Y. Zhang, S.V. Dubonos, I.V. Grigorieva, and A.A. Firsov, "Electric Field Effect in Atomically Thin Carbon Films," *Science*, no. 306, pp. 666–669, 2004.

[3] V.E. Dorgan, M.-H. Bae, and E. Pop, "Mobility and Saturation Velocity in Graphene on $SiO_2$," *Appl.Phys.Lett.*, vol. 97, pp. 082112, 2010.

[4] M.C. Lemme, T.J. Echtermeyer, M. Baus, and H. Kurz, "A Graphene Field Effect Device," *IEEE Electron Device Lett.*, vol. 27, no. 4, pp. 1–12, 2007.

[5] Y.-M. Lin, K.A. Jenkins, A. Valdes-Garcia, J.P. Small, D.B. Farmer, and P. Avouris, "Operation of Graphene Transistors at Gigahertz Frequencies," *Nano Letters*, vol. 9, no. 1, pp. 422–426, 2009.

[6] J. S. Moon, D. Curtis, M. Hu, D. Wong, C. McGuire, P.M. Campbell, G. Jernigan, J.L. Tedesco, B. VanMil, R. Myers-Ward, C. Eddy, and D.K. Gaskill, "Epitaxial-Graphene RF Field-Effect Transistors on Si-Face 6H-SiC Substrates," *IEEE Electron Device Lett.*, vol. 30, no. 6, pp. 650–652, 2009.

[7] I. Meric, C. Dean, A.F. Young, J. Hone, P. Kim, and K.L. Shepard, "Graphene Field-Effect Transistors Based on Boron Nitride Gate Dielectrics," in *IEDM*, Dec. 2010, pp. 23.2.1–23.2.4.

[8] S.-J. Han, Z. Chen, A.A. Bol, and Y. Sun, "Channel-Length-Dependent Transport Behaviors of Graphene Field-Effect Transistors," *IEEE Electron Device Lett.*, vol. 32, no. 6, pp. 812–814, 2011.

[9] M. Engel, M. Steiner, A. Lombardo, A.C. Ferrari, H.v. Loehneysen, P. Avouris, and R. Krupke, "Light-matter Interaction in a Microcavity-controlled Graphene Transistor," *Nature Communications*, vol. 3, pp. 1–6, 2012.

[10] S.A. Imam, S. Sabri, and T. Szkopek, "Low-Frequency Noise and Hysteresis in Graphene Field-Effect Transistors on Oxide," *Micro & Nano Letters*, vol. 5, no. 1, pp. 37–41, 2010.

[11] B. Liu, M. Yang, C. Zhan, Y. Yang, and Y.-C. Yeo, "Bias Temperature Instability (BTI) Characteristics of Graphene Field-Effect Transistors," in *IEEE Trans.VLSI Systems*, 2011, pp. 22–23.

[12] W.J. Liu, X.W. Sun, X.A. Tran, Z. Fang, Z.R. Wang, F. Wang, L. Wu, J.F. Zhang, J. Wei, H.L. Zhu, and H.Y. Yu, "Vth Shift in Single-Layer Graphene Field-Effect Transistors and its Correlation with Raman Inspection," *IEEE Trans.Device and Materials Reliability*, vol. 12, no. 2, pp. 478–481, 2012.

[13] W.J. Liu, X.W. Sun, X.A. Tran, Z. Fang, Z.R. Wang, F. Wang, L. Wu, J.F. Zhang, J. Wei, H.L. Zhu, and H.Y. Yu, "Observation of the Ambient Effect in BTI Characteristics of Back-Gated Single Layer Graphene Field Effect Transistors," *IEEE Trans.Electron Devices*, vol. 60, no. 8, pp. 2682–2686, 2013.

[14] S. Tyaginov, I. Starkov, H. Enichlmair, J.M. Park, Ch. Jungemann, and T. Grasser, "Physics-Based Hot-Carrier Degradation Models," *ECS Transactions*, pp. 321–352, 2011.

[15] S. Vaziri, G. Lupina, A. Paussa, A. D. Smith, C. Henkel, G. Lippert, J. Dabrowski, W. Mehr, M. Östling, and M.C. Lemme, "A Manufacturable Process Integration Approach for Graphene Devices," *Solid-State Electron.*, vol. 84, pp. 185–190, 2013.

[16] Yu.Yu. Illarionov, A.D. Smith, S. Vaziri, M. Ostling, T. Mueller, M.C. Lemme, and T. Grasser, "Bias-Temperature Instability in Single-Layer Graphene Field-Effect Transistors," *Appl.Phys.Lett.*, vol. 105, pp. 143507, 2014.

[17] S. Thiele and F. Schwierz, "Modeling of the Steady State Characteristics of Large-Area Graphene Field-Effect Transistors," *J.Appl.Phys.*, vol. 110, pp. 034506(1–7), 2011.

[18] G. Venugopal, K. Krishnamoorthy, and S.J. Kim, "Investigation of Transfer Characteristics of High Performance Graphene Flakes," *J. Nanosci. Nanotechnol.*, vol. 13, pp. 3515–3518, 2013.

[19] M.I. Katsnelson and K.S. Novoselov, "Graphene: New Bridge between Condensed Matter Physics and Quantum Electrodynamics," *Solid State Comm.*, vol. 143, pp. 3–13, 2007.

[20] D.S. Novikov, "Numbers of Donors and Acceptors from Transport Measurements in Graphene," *Appl.Phys.Lett.*, vol. 91, pp. 102102, 2007.